

RANT: Ant-Inspired Multi-Robot Rainforest Exploration Using Particle Filter Localisation and Virtual Pheromone Coordination

Ameer Alhashemi, Layan Abdulhadi, Karam Abuodeh,
Tala Baghdadi, Suryanarayana Datla

Abstract—This paper presents RANT, an ant-inspired multi-robot exploration framework for noisy, uncertain environments. A team of differential-drive robots navigates a 10×10 m terrain, collects noisy probe measurements of a hidden richness field, and builds local probabilistic maps while the supervisor maintains a global evaluation. RANT combines particle-filter localisation, a behaviour-based controller with gradient-driven hotspot exploitation, and a lightweight no-revisit coordination mechanism based on virtual pheromone blocking. We experimentally analyse how team size, localisation fidelity, and coordination influence coverage, hotspot recall, and redundancy. Results show that particle filtering is essential for reliable hotspot engagement, coordination substantially reduces overlap, and increasing team size improves coverage but yields diminishing returns due to interference.

Index Terms—Multi-robot Exploration, Swarm Robotics, Probabilistic Mapping, Particle-Filter Localisation, Behaviour-Based Control, Gradient-Ascent Search, Virtual Pheromones, Distributed Coordination, Webots Simulation, Environmental Monitoring

I. INTRODUCTION

MULTI-ROBOT exploration is widely used in environmental monitoring, precision agriculture, and large-scale surveying, where several robots must cooperatively explore an area and gather informative measurements [1]. Real deployments rely on noisy GPS, IMU, and wheel odometry, and often operate with limited communication; effective systems therefore favour decentralised, locally reactive controllers [1], [6].

Swarm robotics provides simple decentralised rules, including pheromone-like stigmergy, that improve coverage and reduce interference in multi-agent exploration [4], [5], [11].

A second challenge is localisation: meaningful sampling requires each robot to maintain a stable pose estimate under noise and slip. Particle-filter (Monte Carlo) localisation provides this capability by propagating multiple pose hypotheses and updating them using motion and GPS/heading measurements [6]–[8].

This work introduces **RANT**, an ant-inspired multi-robot exploration framework implemented in Webots. Robots fuse GPS, IMU, and odometry using a particle filter, explore using a behaviour-based controller, and switch to gradient-ascent exploitation when detecting high-richness areas. A lightweight supervisor provides noisy samples from a hidden richness field and broadcasts blocked zones whenever a hotspot is found, discouraging redundant revisits and promoting spatial diversity.

Related Work

Classical exploration frameworks such as frontier-based exploration [1] and occupancy-grid mapping [2] have been extended to multi-robot settings, whereas swarm-based methods emphasise decentralised coordination through local interactions and bio-inspired rules [4], [5], [10], [11]. Distributed gradient climbing and coverage control [9], [12], [13] demonstrate how simple robots can maintain spatial spread while moving toward informative regions.

Monte Carlo localisation is widely used outdoors to mitigate GPS drift and sensor noise [6]–[8], and visual–inertial methods are often used when GPS is degraded, for example under canopy cover [14]. Our work combines these perspectives by analysing how PF localisation, ant-like exploration rules, and virtual-pheromone blocking influence multi-robot coverage.

Contributions

We present (i) a complete Webots-based framework combining PF localisation, gradient exploitation, and virtual-pheromone blocking; (ii) an evaluation of team size, localisation fidelity, and coordination; and (iii) a quantitative study of how these factors shape coverage, hotspot recall, and redundancy, under realistic noise models.

II. SYSTEM OVERVIEW

A. Webots Environment and Hidden Richness Field

The experiments are conducted in a 10×10 m Webots world [15] spanning $[x, y] \in [-5, 5]^2$ with mixed vegetation, rocks, and natural occlusions. The terrain uses Webots’ UnevenTerrain mesh to introduce realistic slopes and height discontinuities, increasing motion and sensing uncertainty.

A hidden scalar “richness” field is maintained by the supervisor on a 50×50 grid,

$$R_g : \{0, \dots, 49\}^2 \rightarrow [0, 1], \quad (1)$$

constructed as a normalised sum of four smooth Gaussian blobs with small perturbations (Fig. 1). Robots never observe R_g directly. During exploration, each robot requests a noisy sample at its current estimated pose; the supervisor maps world coordinates to grid indices, returns the corresponding scalar value, and provides a finite-difference gradient estimate with boundary clamping. These gradient hints inform local exploitation behaviour when robots enter BLOB mode.

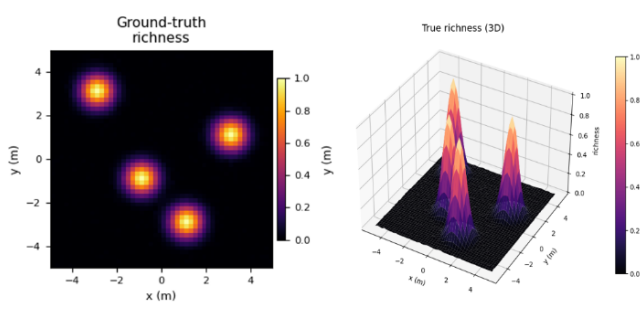


Fig. 1. Supervisor visualisations: (left) ground-truth richness R_g ; (right) 3D true richness.

B. RANT Robot Platform and Sensors

Each agent is a Koala-based differential-drive robot with six wheels arranged as three linked pairs. The controller exposes wheel encoders, GPS, a compass/IMU, and sixteen IR proximity sensors (ds0–ds15). In this section we only outline the sensing suite; the full odometry and noise models are described in Section 3.2.

Odometry: Encoder differences yield left/right wheel displacements and an incremental heading change, following the standard differential-drive model [15]. Wheel accelerations are limited for stable dynamics.

GPS and Heading: GPS and IMU measurements are perturbed with Gaussian noise to emulate realistic outdoor uncertainty:

$$(x_{\text{gps}}, y_{\text{gps}}) = (x, y) + \mathcal{N}(0, 0.02^2), \quad (2)$$

$$\theta_{\text{meas}} = \theta + \mathcal{N}(0, 0.05^2). \quad (3)$$

These noisy readings are fused later by the particle filter.

Obstacle Avoidance: The sixteen IR sensors are arranged in front-left, front-right, and lateral arcs, providing short-range proximity information; the controller uses these arcs for obstacle and wall avoidance as detailed in Section III-C.

C. Environmental Stress Simulation

Three environmental modes are modelled: *clear*, *fog*, and *rain*. The supervisor sets fog visibility, rain intensity, and slip parameters, and stores them in `environment_state.json`. Each robot reads this state and adapts behaviour accordingly.

- **Fog:** reduces speed, increases motion noise and sampling frequency.
- **Rain:** increases slip and motion noise, slightly boosts gradient gains, raises sampling frequency, and introduces radio dropouts.

D. Supervisor, Communication, and Shared Maps

The supervisor maintains the global state of the experiment and exposes a set of shared maps over the 50×50 grid:

- richness field R_g ,
- pheromone map P encoding no-blob-revisit behaviour,
- visited mask V ,

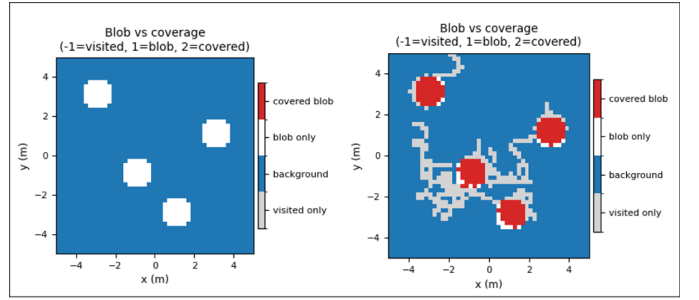


Fig. 2. Supervisor blob-vs-coverage maps before and after a sample $N=5$ run. Red cells denote covered hotspot regions; white cells are hotspot cells not visited; grey traces show robot trajectories; blue is background. The internal mask encodes each grid cell as -1 (visited background), 1 (hotspot), or 2 (covered hotspot).

- blocked mask B marking confirmed hotspot exclusion zones,
- visit-count map C .

These maps form the medium through which robots indirectly influence one another—mirroring ant-style stigmergy. Pheromone accumulation and evaporation shape long-term coverage, while newly declared blocked regions prevent repeated exploitation of discovered hotspots and promote spatial spread across the swarm.

Robots exchange only minimal information with the supervisor through a lightweight message protocol used to support sampling and global coordination:

Robot \rightarrow Supervisor

- `SAMPLE_REQUEST(x, y)` — request a noisy richness reading and gradient;
- `BULLSEYE` — announce a detected hotspot centre;
- `TELEMETRY` — send particle-filter pose estimates.

Supervisor \rightarrow Robot

- `SAMPLE_RESPONSE($R, \nabla R$)` — return noisy values;
- `BLOCK(x, y, r)` — publish a circular forbidden region after a hotspot is confirmed;
- `STOP_ALL` — terminate the run after four hotspots are found.

Each confirmed sample at cell (i, j) updates the shared maps:

$$P_{ij} \leftarrow P_{ij} + 1, \quad C_{ij} \leftarrow C_{ij} + 1, \quad V_{ij} \leftarrow 1, \quad (4)$$

with pheromone evaporating as

$$P_{ij}(t+1) = 0.995 P_{ij}(t). \quad (5)$$

When a robot reports a hotspot, the supervisor inserts a blocked disc into B and increments a global hotspot counter. Once four hotspots have been validated, it broadcasts `STOP_ALL` and constructs a blob-vs-coverage mask (Fig. 2) summarising which hotspot cells were visited and how trajectories intersected the ground-truth richness field.

III. ALGORITHMS

This section outlines the main algorithms in RANT: construction of the hidden richness field and local belief maps, particle-filter localisation, the behaviour-based controller, and

simple environmental adaptation. For each component we briefly state cost, convergence behaviour, and main failure modes.

All results were generated using fixed evaluation protocols across runs. Key environment and algorithm parameters are recorded in the experiment configuration files used for evaluation.

A. Richness Field, Gradients, and Local Belief Maps

The supervisor represents the hidden richness field R_g on a 50×50 grid over the 10×10 m arena. It is constructed as a mixture of four Gaussian bumps,

$$R_g(j, i) = \sum_{k=1}^4 \exp\left(-\frac{(i - \mu_{x,k})^2 + (j - \mu_{y,k})^2}{2\sigma^2}\right), \quad (6)$$

normalised to $[0, 1]$ and perturbed with small noise. Robots never see R_g directly; they issue `SAMPLE_REQUEST`(x, y) messages, which the supervisor maps to indices (i, j) and answers with a noisy scalar sample and a finite-difference gradient estimate.

World coordinates (x, y) are mapped linearly to grid indices $(i, j) \in \{0, \dots, 49\}^2$ over $[x_{\min}, x_{\max}] \times [y_{\min}, y_{\max}]$. Central differences with boundary clamping approximate the gradient:

$$\frac{\partial R}{\partial x} \approx \frac{R_g[j, i+1] - R_g[j, i-1]}{2 \Delta x}, \quad (7)$$

$$\frac{\partial R}{\partial y} \approx \frac{R_g[j+1, i] - R_g[j-1, i]}{2 \Delta y} \quad (8)$$

Cells inside supervisor-declared blocked regions return $R=0$ and $\nabla R=0$, so confirmed hotspots become repulsive for the goal selector.

Each robot maintains a small local belief grid (40×40 cells at $\Delta = 0.1$ m resolution) storing private, running means of sampled richness for offline inspection. For a sample with measured richness R_{meas} at (x, y) inside the window, the corresponding cell (i, j) stores an integer visit count c_{ij} and a running mean M_{ij} ,

$$c_{ij} \leftarrow c_{ij} + 1, \quad M_{ij} \leftarrow \frac{c_{ij} M_{ij} + R_{\text{meas}}}{c_{ij} + 1}.$$

Cost, convergence, failure modes. R_g is precomputed once in $O(G_x G_y)$ and each query is $O(1)$. Running means converge under unbiased noise, but boundary clamping, flat gradients, and localisation drift can blur reconstructed blobs.

B. Particle-Filter Localisation

Each robot runs a particle filter (PF) with $N = 150$ particles to estimate its pose (x, y, θ) . On the first valid GPS fix, particles are initialised in a Gaussian window around the GPS position and IMU heading with uniform weights.

At each control cycle the PF executes a standard predict-update-resample sequence. The motion model uses odometry-derived forward motion d and rotation $\Delta\theta$:

$$\theta'_i = \theta_i + \Delta\theta + \mathcal{N}(0, \sigma_\theta^2),$$

$$x'_i = x_i + d \sin \theta'_i + \mathcal{N}(0, \sigma_d^2),$$

$$y'_i = y_i + d \cos \theta'_i + \mathcal{N}(0, \sigma_d^2),$$

with σ_d and σ_θ proportional to $|d|$ and $|\Delta\theta|$ to capture slip and unmodelled dynamics.

The measurement update uses the noisy GPS and heading measurements defined in Section II B. For each particle (x_i, y_i, θ_i) we evaluate a positional likelihood with standard deviation σ_{gps} and, when heading is available, a heading likelihood with standard deviation σ_θ . Final weights $w_i = w_i^{\text{pos}} w_i^\theta$ are normalised so that $\sum_i w_i = 1$, and the pose estimate is taken as the weighted mean

$$(x_{\text{est}}, y_{\text{est}}, \theta_{\text{est}}) = \sum_i w_i (x_i, y_i, \theta_i). \quad (9)$$

To avoid particle impoverishment we monitor the effective particle count

$$N_{\text{eff}} = \frac{1}{\sum_i w_i^2}, \quad (10)$$

and trigger systematic resampling whenever $N_{\text{eff}} < \alpha N$ with $\alpha = 0.95$.

For later evaluation the controller logs the instantaneous localisation error

$$e(t) = \sqrt{(x_{\text{true}} - x_{\text{est}})^2 + (y_{\text{true}} - y_{\text{est}})^2}, \quad (11)$$

from which MAE, RMSE, and maximum error are computed in Section V-B.

Cost, convergence, failure modes. Each update is $O(N)$. With intermittent GPS the cloud quickly settles and then shows expand-collapse cycles; if GPS degrades or resampling is too infrequent the cloud diffuses and drift grows to metre scale.

C. Behaviour-Based Controller and Obstacle Handling

Each robot runs a three-mode finite-state controller with an emergency *unstuck* routine. Commands are issued as forward speed v_{cmd} and angular velocity w_{cmd} , then converted to wheel speeds with acceleration limits.

EXPLORE is a biased random walk: every ~ 0.8 s a new exploratory term w_{osc} is sampled from a zero-mean Gaussian while forward speed stays near `BASE_FWD`. Steering combines (i) the random term, (ii) obstacle and corner avoidance from the 16 IR sensors, (iii) soft wall recentering, (iv) a small radial-band dispersion bias, and (v) repulsion from locally stored blob centres and supervisor-declared blocked discs, which act as soft virtual obstacles.

BLOB mode performs local search around promising samples. EXPLORE switches to BLOB once the best observed richness exceeds `BLOB_ENTER_VAL`. If a best point (x_b, y_b) is known, steering tracks the bearing $\theta_{\text{target}} = \text{atan2}(y_b - y, x_b - x)$ with a bounded proportional heading correction; otherwise the supervisor's gradient direction is used. Forward speed decreases with heading error, and an edge-escape term prevents sliding along blob boundaries. BLOB terminates when values fall below `BLOB_EXIT_VAL` for `BLOB_EXIT_COUNT` consecutive samples, after which the blob centre is added to a private forbidden list.

RECOVER is entered after leaving a blob or declaring a bullseye. The robot drives mostly straight at `RECOVER_SPEED` using only obstacle, wall, and no-revisit

corrections, until it has moved at least RECOVER_MIN_DIST or a timeout occurs. This prevents tight circling near discovered hotspots. When global blocking is enabled, the newly confirmed blob centre is added to the supervisor’s blocked mask, so RECOVER automatically treats the blob region as a repulsive zone; with blocking disabled, robots simply move away without any long-term repulsion.

An **unstuck** manoeuvre is triggered if the robot’s pose has not changed more than STUCK_POS_EPS over STUCK_TIME. It executes a short reverse-and-turn followed by a forward turn, temporarily overriding all other steering and clearing rare deadlocks.

Obstacle and wall handling use the 16 IR sensors grouped into front-right, front-left, and lateral arcs. If either front arc exceeds a threshold, a turning command w_{obs} is generated away from the stronger side and forward speed is reduced as readings approach a hard-stop level; a “corner” condition (both arcs high) briefly boosts turn rate. Side sensors provide gentle lateral repulsion that keeps the robot from grazing walls.

Cost, convergence, failure modes. Closed-loop behaviour typically yields wide-area coverage with repeated convergence toward unexplored hotspots until the supervisor triggers STOP_ALL. Transient jitter from noisy side sensors or tight corners is normally resolved by RECOVER or the unstuck routine within a few seconds. Tuning of virtual blocks is critical: overly large BLOCK_RADIUS_M can render regions effectively inaccessible and depress coverage, whereas very small radii or weak pheromone penalties produce behaviour almost indistinguishable from the uncoordinated baseline, offering little reduction in redundancy.

D. Environmental Adaptation

Robots adapt controller gains to fog and rain by reducing speed, increasing motion noise, adjusting sampling frequency, and injecting radio dropouts under heavy rain. In clear conditions they use the nominal maximum speed and a 0.5s sampling period; fog reduces speed by roughly 20–25% and increases sample interval, while rain halves the maximum speed, slightly increases sampling frequency, and introduces frequent communication drops. These changes primarily raise traversal time rather than fundamentally altering the controller logic.

Cost, convergence, failure modes. Adaptation is $O(1)$ per step and mainly affects traversal time: heavy fog or extreme slip slow coverage and delay recovery from wall contacts, but in our runs did not produce catastrophic failures.

IV. EXPERIMENTAL EVALUATION

We evaluate how team size, localisation fidelity, and pheromone-based coordination affect exploration performance and mapping accuracy. All runs use the same 10×10 m Webots arena, richness field, and noise models.

A. Experiment 1: Effect of Team Size on Coverage and Mapping Time

Objective. Quantify how increasing team size affects spatial coverage, hotspot detection, and redundancy.

Setup. We compare teams of size $N \in \{1, 3, 5\}$. All robots use particle-filter localisation, the EXPLORE/BLOB/RECOVER controller, fixed, slightly offset starting poses in a common spawn region, and the same richness field with four Gaussian blobs.

Hypotheses.

- **H1a (coverage and recall):** Increasing N increases world coverage and blob recall (fraction of blob cells visited).
- **H1b (redundancy):** Pheromone-like no-revisit and blocked-zone coordination prevent redundancy from growing linearly with N , so multi-robot runs remain more sample-efficient than a naïve “more robots = more overlap” baseline.

Metrics. For each N we measure:

- world coverage (fraction of grid cells ever visited) and blob recall;
- precision and F1 on coverage, treating blob cells as positives;
- blob detection rate (blobs with at least one visited cell);
- redundancy,

$$\text{redundancy} = 1 - \frac{\text{unique visited cells}}{\text{total samples}}. \quad (12)$$

The four blobs occupy 180 of 2500 cells ($\approx 7.2\%$), so a purely uniform sampler would achieve only $\sim 7\%$ precision.

B. Experiment 2: Impact of Localisation Fidelity

Objective. Assess how localisation fidelity affects (i) the internal consistency of the particle filter and (ii) the ability of robots to detect and exploit hotspots.

Setup. We reuse the arena, richness field, and team size from Experiment 1 and compare:

- 1) **PF-enabled (PF-on)**
- 2) **PF-disabled (PF-off)**

Hypotheses.

- **H2a (hotspot reactivity):** PF-enabled robots will enter BLOB mode and dwell inside hotspots; PF-disabled robots will traverse hotspots without reacting.
- **H2b (sampling and coverage):** PF-enabled runs will generate many valid SAMPLE_REQUESTs and dense sampling around hotspots, whereas PF-disabled runs will produce no samples and no coverage in supervisor maps.

Metrics and assessment tools. For each condition we analyse:

- console traces of control and SAMPLE_AT (finite values vs. (nan, nan));
- mode transitions (EXPLORE vs. BLOB/RECOVER);
- counts and spatial distribution of SAMPLE_REQUESTs and visited cells;
- instantaneous localisation error (Eq. (11)), from which MAE, RMSE, and Max error are derived;
- supervisor particle-cloud visualisations: stable filters show expand-collapse cycles as GPS updates arrive, whereas unstable filters diffuse and drift away from the true pose.

C. Experiment 3: Influence of Pheromone Blocking and Coordination

Objective. Evaluate whether virtual pheromone blocking (ENABLE_GLOBAL_BLOCKING) reduces redundant sampling and improves spatial spread for a fixed team of five robots.

Setup. We fix the environment, supervisor configuration, and team size to match the final implementation. All robots use particle-filter localisation and the EXPLORE/BLOB/RECOVER controller. We set $N = 5$ to evaluate coordination effects under realistic multi-robot interference. Two conditions are compared:

- 1) **Coordination ON:** global blocked zones and pheromone penalties are applied after each BULLSEYE.
- 2) **Coordination OFF:** no global blocking and no long-term repulsion; BLOCK messages are ignored.

Hypotheses.

- **H3a (redundancy):** Blocking and no-revisit should reduce the fraction of samples taken on already-visited cells.
- **H3b (hotspot discovery):** Coordination should maintain or improve blob recall and the number of distinct blobs discovered.

Metrics. For coordination ON and OFF we compute:

- world coverage and blob recall;
- precision and F1 on coverage (blob cells as positives);
- blob detection rate (blobs with at least one visited cell);
- redundancy Eq. (12)
- visit-entropy and, for coordination ON, the fraction of cells marked as blocked in the global blocked mask.

V. RESULTS AND DISCUSSION

This section presents the outcomes of the three experiments. Across all runs, we focus on coverage, hotspot recall, localisation error, and sampling redundancy.

A. Effect of Team Size

a) Qualitative behaviour: Visit heatmaps (Fig. 3) show increased exploration range with larger teams, but also more concentrated revisits around hotspots at $N = 5$. Figure 4 shows the corresponding blob-vs-coverage masks. As expected, increasing the number of robots improves exploration efficiency and hotspot discovery. In the five-robot run, the supervisor’s STOP_ALL condition (all four blobs detected) fired at $t = 356$ s. By contrast, the $N = 1$ and $N = 3$ runs never reached this condition within the same simulation horizon, leaving one or more blobs undiscovered. Larger teams clearly reduce time-to-detection.

b) Quantitative metrics: Quantitatively, Table I shows that increasing team size from $N = 1$ to $N = 5$ increases world coverage from 8.5% to 18.1% and blob recall from 20.0% to 65.6%. Precision improves sharply from $N = 1$ to $N = 3$, but then drops slightly at $N = 5$: the larger team discovers more blob cells overall, but also generates more samples in background regions around them. F1 follows a similar pattern: $N = 3$ offers a good balance of coverage

TABLE I
COVERAGE AND HOTSPOT METRICS FOR DIFFERENT TEAM SIZES

Metric	$N = 1$	$N = 3$	$N = 5$
World coverage (%)	8.5	9.8	18.1
Blob recall (%)	20.0	46.7	65.6
Precision on coverage (%)	17.0	34.4	26.1
F1 score	0.184	0.396	0.373
Blobs detected (≥ 1 cell)	1/4	3/4	4/4
Time to STOP_ALL (s)	–	–	356

Time to STOP_ALL is only defined when the supervisor’s stopping condition (all four blobs detected) is met. For $N = 1$ and $N = 3$ the runs reached the simulation time limit without satisfying this condition; these entries are therefore marked “–”.

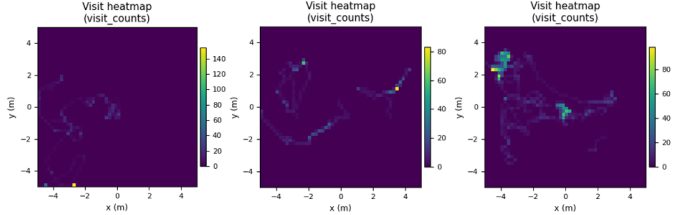


Fig. 3. Visit-count heatmaps for team sizes $N = \{1, 3, 5\}$ (left to right). Brighter regions indicate cells visited more frequently. With more robots the explored area grows and hotspots are detected earlier, but redundant sampling becomes more localised around blob regions, reflecting increased interference at higher team sizes.

and focus, while $N = 5$ trades a small drop in F1 for full blob detection and higher absolute recall.

c) Failure modes: For $N = 1$ and $N = 3$, limited spatial reach and stochastic drift can prevent the team from ever entering all blob regions within the fixed time horizon, so STOP_ALL is not triggered. At $N = 5$, although all blobs are detected, stronger local interference produces revisit bands around blob boundaries where multiple robots oscillate through the same high-richness region.

B. Localisation Fidelity: PF Behaviour and PF-On vs PF-Off

a) Qualitative behaviour: Figure 5 illustrates two characteristic PF outcomes during a five-robot run. In the healthy case, the particle cloud expands under motion and collapses when GPS updates agree with odometry, so robots maintain tight pose estimates and repeatedly enter BLOB mode over hotspots. In the unstable case (mis-tuned resampling), the cloud spreads but never collapses: weights remain almost flat, drift grows to metre scale, and robots start making visibly wrong decisions (e.g. incorrect avoidance or missing hotspots). In the PF-disabled ablation, control_x and SAMPLE_AT remain (nan, nan) and robots stay in EXPLORE, traversing blob regions without reacting; visit-count maps are essentially empty.

b) Quantitative metrics: Using the error metric in Eq. (11), a successful five-robot run (all hotspots found) with $\alpha = 0.7$ achieved:

$$\text{MAE} = 0.133 \text{ m}, \quad \text{RMSE} = 0.208 \text{ m}, \quad \text{Max} = 1.105 \text{ m}.$$

An unstable run with a drifting PF yielded:

$$\text{MAE} = 0.363 \text{ m}, \quad \text{RMSE} = 0.914 \text{ m}, \quad \text{Max} = 3.783 \text{ m},$$

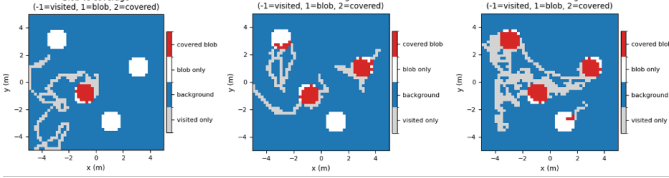


Fig. 4. Blob-vs-coverage maps for team sizes $N = \{1, 3, 5\}$ (left to right). In the $N = 5$ case, the final blob appears only partially covered because the supervisor terminated the run immediately after all four hotspots were detected, before additional samples could accumulate around that region.

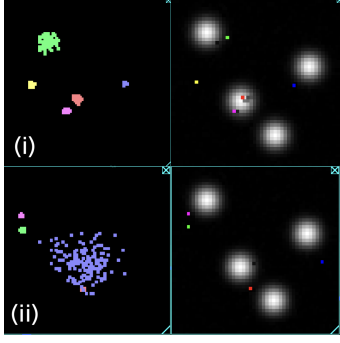


Fig. 5. Illustrative particle-filter behaviour during a five-robot run. The left panel shows live particle clouds; the right panel shows true robot poses overlaid on the richness map. Stable filters maintain tight clouds around true poses; unstable filters spread and drift, producing large localisation error.

showing how a single diverging filter can dominate team-level localisation error and distort behaviour. In the PF-off ablation, errors are undefined and no valid samples are ever logged, which matches the visually empty heatmaps.

c) *Failure modes*: These results confirm that RANT’s mapping pipeline is structurally dependent on a coherent PF estimate: with mis-tuned resampling or degraded GPS the particle cloud drifts, samples never register, and hotspots remain effectively invisible, even though robots continue to move.

C. Impact of Pheromone-Based Coordination

a) *Qualitative behaviour*: The virtual pheromone grid and blocked-mask coordination were evaluated by comparing runs with coordination enabled versus disabled in a five-robot team. Without pheromone guidance, robots frequently revisit already sampled regions, especially around strong hotspots. This raises redundancy and slows the discovery of new informative areas. With coordination enabled, robots show a clear tendency to disperse: evaporation causes old paths to fade, the goal selector penalises recently explored regions, and blocked discs prevent repeated exploitation of confirmed hotspots.

b) *Quantitative metrics*: Table II quantifies these effects. Coordination nearly doubles blob recall ($33.9\% \rightarrow 65.6\%$) and increases world coverage and F1 score while maintaining full hotspot detection. Although absolute precision remains modest because robots must still survey large background regions, coordination improves precision from 16.7% to 26.1% . Combined with the higher recall and F1, this indicates that blocked zones and no-revisit logic make the swarm’s sampling more

TABLE II
EFFECT OF PHEROMONE-BASED COORDINATION ON MAPPING QUALITY
(5 ROBOTS)

Metric	Coord. ON	Coord. OFF
Blob cells (total)	180	180
Blob cells covered	118	61
Blob recall (%)	65.6	33.9
Covered cells (any)	452	366
World coverage (%)	18.1	14.6
Precision on coverage (%)	26.1	16.7
Accuracy (whole world, %)	84.2	83.0
F1 score	0.373	0.223
Blobs detected (≥ 1 cell)	4/4	4/4

focused on blob cells rather than simply amplifying random exploration.

c) *Failure modes*: Even with coordination enabled, virtual pheromones do not eliminate all redundant sampling: around very strong hotspots, robots can still cluster briefly on blob boundaries before repulsion and evaporation pull them apart. With coordination disabled, these effects are amplified, redundancy grows, and the time to discover new blobs increases.

Overall, pheromone-based coordination improves coverage uniformity, reduces redundant sampling, and makes better use of multi-robot deployments without requiring explicit inter-robot communication.

VI. CONCLUSION

RANT demonstrates that a small team of ant-inspired robots, equipped with particle-filter localisation and simple virtual-pheromone rules, can reliably discover and exploit hidden hotspots in a noisy, partially structured environment. Larger teams accelerate hotspot detection but suffer diminishing returns due to interference; localisation fidelity is structurally required for mapping, and pheromone-based blocking improves coverage quality by reducing redundant sampling and spreading robots across the arena.

The current GPS+IMU Webots proxy best reflects open or moderately occluded sites; dense canopy would require additional visual-inertial or landmark cues to keep drift bounded. The simulated world also simplifies vegetation, dynamics, communication, and weather, and coordination is mediated by a central supervisor rather than fully distributed communication.

Future work includes richer sensing (e.g. visual-inertial odometry, shared local maps), more realistic communication and failure models, and field trials on hardware platforms. This study is simulation-based and intended to isolate the effect of coordination and localisation assumptions under controlled conditions; transferring to physical robots will require additional modelling of sensing and communication constraints. Exploring alternative bio-inspired coordination mechanisms or learning-based controllers would help test how far simple ant-like rules can be pushed in large-scale, real-world monitoring tasks.

REFERENCES

- [1] B. Yamauchi, "Frontier-based exploration using multiple robots," in *Proc. 2nd Int. Conf. Autonomous Agents (AGENTS '98)*, ACM, New York, NY, USA, 1998. doi: 10.1145/280765.280773.
- [2] A. Elfes, "Sonar-based real-world mapping and navigation," *IEEE J. Robot. Autom.*, vol. 3, no. 3, pp. 249–265, Jun. 1987, doi: 10.1109/JRA.1987.1087096.
- [3] F. Iida, "Autonomous Robots: From Biological Inspiration to Implementation and Control. George A. Bekey," *Artificial Life*, vol. 13, no. 4, pp. 419–421, Oct. 2007, doi: 10.1162/artl.2007.13.4.419.
- [4] E. Şahin, S. Girgin, L. Bayindir, and A. E. Turgut, "Swarm robotics," in *Swarm Intelligence*, C. Blum and D. Merkle, Eds. Berlin, Heidelberg: Springer, 2008. doi: 10.1007/978-3-540-74089-6_3.
- [5] M. Dorigo, M. Birattari, and T. Stützle, "Ant colony optimization," *IEEE Comput. Intell. Mag.*, vol. 1, pp. 28–39, 2006, doi: 10.1109/MCI.2006.329691.
- [6] S. Thrun, W. Burgard, and D. Fox, *Probabilistic Robotics*. MIT Press, 2005.
- [7] S. Thrun, "Particle filters in robotics," in *Proc. 18th Conf. Uncertainty in Artificial Intelligence (UAI '02)*, Morgan Kaufmann, San Francisco, CA, USA, 2002, pp. 511–518.
- [8] F. Dellaert, D. Fox, W. Burgard, and S. Thrun, "Monte Carlo localization for mobile robots," in *Proc. IEEE Int. Conf. Robot. Autom.*, vol. 2, 1999, pp. 1322–1328, doi: 10.1109/ROBOT.1999.772544.
- [9] P. Ogren, E. Fiorelli, and N. E. Leonard, "Cooperative control of mobile sensor networks: Adaptive gradient climbing in a distributed environment," *IEEE Trans. Autom. Control*, vol. 49, no. 8, pp. 1292–1302, Aug. 2004, doi: 10.1109/TAC.2004.832203.
- [10] S. Nouyan, A. Campo, and M. Dorigo, "Path formation in a robot swarm," *Swarm Intell.*, vol. 2, pp. 1–23, 2008. doi: 10.1007/s11721-007-0009-6.
- [11] Krieger, M., Billeter, JB. & Keller, L. Ant-like task allocation and recruitment in cooperative robots. *Nature* 406, 992–995 (2000). <https://doi.org/10.1038/35023164>.
- [12] H. Choset, "Coverage for robotics – A survey of recent results," *Annals of Mathematics and Artificial Intelligence*, 2001.
- [13] E. Fiorelli, N. E. Leonard, P. Bhatta et al., "Multi-agent gradient climbing for environmental sampling," in *Proc. IEEE Conf. Decision and Control (CDC)*, 2003.
- [14] S. Weiss, M. Achtelik, L. Kneip et al., "Real-time onboard visual–inertial state estimation and self-calibration of MAVs in unknown environments," in *Proc. IEEE Int. Conf. Robotics and Automation (ICRA)*, 2012.
- [15] O. Michel, "Cyberbotics Ltd. Webots™: Professional Mobile Robot Simulation," *Int. J. of Advanced Robotic Systems*, 2004.